Trimethyltin-Mediated Covalent Gold−Carbon Bond Formation

Arunabh Batra,[†] Gregor Kladnik,[∇,#] Narjes Gorjizadeh,[§,‖] Jeffrey Meisner,[⊥] Michael Steigerwald,[⊥] Colin Nuckolls,[⊥] Su Ying Quek,*,[§,‖] Dean Cvetko,[‡,∇] Alberto Morgante,*,[∇,#] and Latha Venkataraman*,[†]

[†]Department of Applied Physics and Applied Mathematics and [⊥]Department of Chemistry, Columbia University, New York, New York 10027, United States

[‡]Department of Physics, University of Ljubljana, SI-1000 Ljubljana, Slovenia

[∇]CNR-IOM Laboratorio Nazionale TASC, I-34012 Trieste, Italy

[§]Department of Physics, National University of Singapore, 117551 Singapore

[‖]Institute of High Performance Computing, Agency for Science, Technology and Research−A*STAR, 138632 Singapore

[#]Department of Physics, University of Trieste, I-34127 Trieste, Italy

S *Supporting Information*

ABSTRACT: We study the formation of covalent gold−carbon bonds in benzyltrimethylstannane ($C_{10}H_{16}Sn$) deposited on Au in ultra-high-vacuum conditions. Through X-ray photoemission spectroscopy and X-ray absorption measurements, we find that the molecule fragments at the Sn−benzyl bond when exposed to Au surfaces at temperatures as low as −110 °C. The resulting benzyl species is stabilized by the presence of Au(111) but only forms covalent Au−C bonds on more reactive Au surfaces like Au(110). We also present spectroscopic proof for the existence of an electronic "gateway" state localized on the Au−C bond that is responsible for its unique electronic properties. Finally, we use DFT-based nudged elastic band calculations to elucidate the crucial role played by the under-coordinated Au surface in the formation of Au−C bonds.

A well-defined, robust, metal−organic contact is fundamental in organic electronics systems. Such contacts not only mechanically anchor the organic components but also define and enhance the electronic characteristics of devices. One popular type of contact is the gold−thiol bond;[1] its covalent nature provides superior mechanical stability and high electronic transparency.[2] Au−S bonds can form well-packed, uniform self-assembled monolayers[3] however, the nonspecific nature of the Au−S bond means that well-defined,[4] uniform molecule−metal geometries, and consequently electronic properties,[5] are difficult to obtain.[6] Further problems with thermal stability and degradation due to oxidation[7] have led researchers to explore alternatives, such as a variety of donor−acceptor bonds[8] and recently covalent gold−carbon bonds.[9] Direct Au−C bonds are often formed electrochemically by the reduction of aryldiazonium salts in solution.[10] Covalent σ-coupled Au−C bonds have also been formed using terminal alkynes,[11] organomercury salts,[12] trimethylsilyl linkers,[13] and trimethyltin leaving groups.[9]

Recently, Chen et al.[14] demonstrated the use of benzyltrimethyltin molecules to form Au−C bonds that can couple into the π-system of a conjugated molecular backbone. In single-molecule experiments, they show near-resonant molecular

conductance, nearly 100 times that of molecules with conventional linker groups.[14] The electronic properties of these π-coupled Au−C bonds have also been shown to facilitate desirable thermoelectric characteristics[15] and have been integrated into tunable molecular diode designs.[16] Theoretical calculations suggest that a hybridized gold−molecule "gateway" state,[14,16] localized on the Au−C bond, may be responsible for many of the unique electronic properties of these π-coupled systems, though there is no experimental evidence for the existence of such a state.

Here we study the formation of Au−C bonds using benzyltrimethylstannane ($C_{10}H_{16}Sn$) molecules on a variety of Au surfaces in ultra-high-vacuum (UHV) conditions. In contrast with studies conducted on similar systems in organic solvent solutions in ambient conditions,[9,14] this UHV study allows us to isolate the role of Au in such reactions. Through X-ray photoemission spectroscopy (XPS) measurements, we show that, even at temperatures as low as −110 °C in the presence of a Au substrate, $C_{10}H_{16}Sn$ cleaves at the Sn−C bond to form trimethyltin (C_3H_9Sn) and benzyl (C_7H_7) species. The resulting trimethyltin fragments readily form Sn−Au bonds on all surfaces, while the fate of the benzyl species is determined by the reactivity of the Au surface. On Au(111), XPS core-level shifts point to the formation of a surface-stabilized benzyl radical. In contrast, XPS on Au(110) shows no such shift; instead, near-edge X-ray absorption fine structure spectroscopy (NEXAFS) on this surface shows the formation of a Au−C bond with a well-hybridized electronic "gap" state. Finally, through density functional theory (DFT)-based implementations of nudged elastic band (NEB) calculations,[17] we determine a reaction pathway for covalent Au−C bond formation that allows us to understand the essential role played by under-coordinated Au surfaces in facilitating these reactions.

We characterize the cleavage of benzyltrimethylstannane (Figure 1a) using XPS measurements of monolayer films of the molecule deposited on Au(111), Au(110), and sputtered Au surfaces, carried out at the ALOISA/HASPES beamline (Elettra Synchrotron, Trieste).[18] Details of sample preparation are given in the SI. Briefly, we deposit Benzyltrimethylstannane synthe-
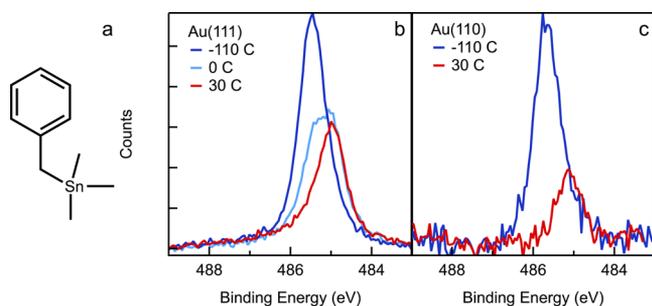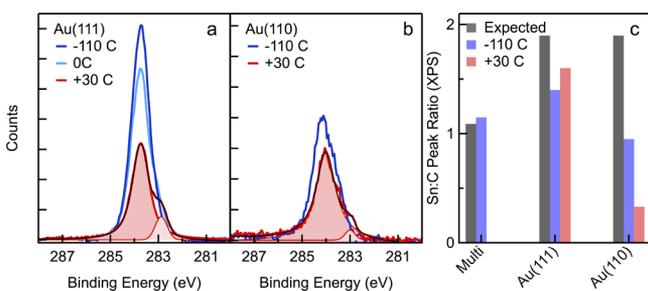
Figure 1. (a) Benzyltrimethylstannane molecular structure. (b,c) XPS of Sn 3d$_{5/2}$ for a monolayer (b) on Au(111) at −110 (dark blue), 0 (light blue), and +30 °C (red) and (c) on Au(110) at −110 (dark blue) and +30 °C (red).

sized using previously reported methods[14] on cleaned Au substrates for the XPS and NEXAFS measurements.

We first compare the XPS signal of Sn 3d$_{5/2}$ core levels (Figure 1b,c) as a function of substrate temperature on Au(111) and Au(110). For Au(111) at −110 °C (dark blue, Figure 1b), the Sn 3d$_{5/2}$ peak is a broad feature centered at 485.4 eV. As the substrate temperature is raised to 0 °C (light blue), the Sn 3d$_{5/2}$ signal decreases dramatically, and a second lower-binding component arises at 485.0 eV. At 30 °C (red, Figure 1b), the lower-binding component dominates. A similar trend is seen in Au(110) (Figure 1c), with a shift of 0.4 eV in Sn 3d$_{5/2}$ and an even more dramatic loss of Sn. The downward core-level shift of 0.4 eV between the original and new peaks corresponds to the chemical shift between Sn−C and Sn−Au bonds,[19] pointing to the conversion of trimethyltin fragments into Au-bound trimethyltin upon heating on both Au(111) and Au(110).

Figure 2a,b compares the C 1s peaks for the Au(111)and Au(110) surfaces. For Au(111) (Figure 2a), we see a broad C 1s peak at 283.8 eV with the substrate at −110 °C (dark blue). As substrate temperature is raised to 0 °C (light blue), some C signal is lost from the original peak, and a lower-binding peak emerges as a shoulder at 282.9 eV. At 30 °C, the 282.9 eV peak in C 1s becomes more prominent. This new peak, shifted to lower binding energy by 0.9 eV from the main peak, can be attributed to a C 1s electron of a surface-stabilized benzyl radical on Au(111), as has been shown by calculations.[20] In addition, we find that the XPS ratio for the two C species (283.8 eV C 1s to 282.9 eV C 1s peak) at 30 °C corresponds to a stoichiometric ratio of 8:1, consistent with the expected ratio for a surface-stabilized benzyl

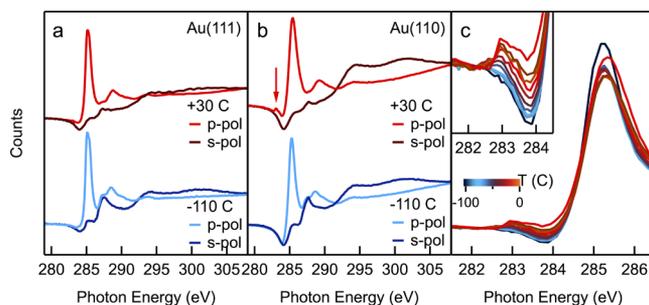radical once the desorption of trimethyltin is accounted for (see SI for details).

On Au(110) (Figure 2b) we find that, while there is still a loss of C, the peak that is shifted by 0.9 eV from the main peak is significantly reduced. Since the missing row reconstructed Au(110) surface has 111 facets exposed at monatomic steps, we attribute the small signal at this binding energy to the benzyl radical that forms on these facets. This indicates that a surface-stabilized radical is not as predominant on Au(110) as it is on Au(111). Instead, a covalent Au−C bond is formed that, based on previous studies, shows a very minimal XPS shift.[12,21] Further evidence for the formation of covalent Au−C bonds on Au(110) is presented below.

We now examine the overall Sn:C signal ratio in Figure 2c, which shows calculated (shaded bars, see SI for details) Sn:C XPS signal ratios against measured values for multilayer films and monolayers on Au(111) and Au(110). In contrast with the multilayer, where measured and expected Sn:C ratios agree well, monolayers on Au(111) and Au(110) show less Sn than expected at all temperatures. These data point to fragmentation of the original molecule into a purely C-containing benzyl fragment and a trimethyltin fragment, with different affinities for the Au surfaces. The proportionally lower Sn signal on the Au(110) is in agreement with previous theoretical studies showing that trimethyltin prefers to bind on flat Au.[9]

We turn next to NEXAFS spectra of the C K-edge to study the unoccupied energy levels of the cleaved molecular fragments on Au(111) and Au(110). NEXAFS spectra are collected with incident photon energy between 280 and 310 eV, with the electric field polarization either parallel (s-pol) or perpendicular (p-pol) to the sample, and with a beam incidence angle of 6°. Figure 3a,b shows NEXAFS measurements for monolayers of benzyltrimethylstannane on Au(111) and Au(110), respectively. At −110 °C (blue curves), the NEXAFS spectra are dominated by a prominent π* peak[22] at 285 eV in p-pol (light colors). This "dichroism" in NEXAFS indicates that the molecules lie with the benzene rings relatively flat on both substrates. We see further that the NEXAFS spectra on Au(110) are quite different from those on Au(111). First, the π* peak on Au(110) is significantly broadened for the monolayer film at +30 °C, in contrast to both the low-temperature Au(110) and the Au(111) spectra (shown in detail in Figure S1). This broadening indicates that the lowest unoccupied molecular orbital (LUMO) is better coupled to the Au surface for the 30 °C film on Au(110). Second, we find an additional prominent peak emerging around 283 eV (red arrow, Figure 3b). The asymmetry of the peak, with a sharp increase at

Figure 2. (a,b) C 1s XPS of a monolayer of C$_{10}$H$_{16}$Sn (a) on Au(111) at −110 (dark blue), 0 (light blue), and +30 °C (red) and (b) on Au(110) at −110 (dark blue) and +30 °C (red). Black lines represent a best fit of the +30 °C XPS signal using two Voigt functions (filled red). (c) Ratio of XPS peak areas for Sn:C at −110 (blue bars) and +30 °C (red bars) for a multilayer film and monolayer films on Au(111) and Au(110). Gray bars represent the expected ratio of Sn:C for intact C$_{10}$H$_{16}$Sn.

Figure 3. Carbon K-edge NEXAFS taken in s-pol (dark colors) and p-pol (light colors) of a monolayer on (a) Au(111) at −110 (blue) and +30 °C (red) and (b) on Au(110) at −110 (blue) and +30 °C (red). (c) NEXAFS taken in p-pol on a sputtered Au surface, as a function of temperature. All NEXAFS spectra shown here are raw data.

the low-energy side, resembles the step shape and energy width of the Fermi distribution.

Simulated NEXAFS calculations on a Au_1−benzyl molecule (see SI for details) show that the pre-edge feature occurs due to the excitation of a core-level electron from the C atom bound to Au to the LUMO of the Au_1−benzyl species. This LUMO, now singly occupied, extends spatially to the benzyl C and the Au−C bond, suggesting that the covalent Au−C bond is well hybridized with the LUMO of the benzyl. Additionally, theory shows that this state is oriented along the Au−C bond direction; this theoretical evidence, along with the fact that the pre-edge feature is absent in s-pol (dark red, Figure 3b), shows that the Au−C bond is perpendicular to the surface. The pre-edge peak corresponding to the "gap state" seen in C K-edge NEXAFS is absent in Au(111), indicating that covalent Au−C bonds form preferentially on under-coordinated surfaces.

To test the dependence of this feature on surface coordination, molecules were deposited on a cold-sputtered Au surface, prepared by Ar sputtering of a Au(111) substrate maintained at −110 °C. After molecular deposition, rapid NEXAFS scans in p-pol were measured as a function of increasing substrate temperature. Figure 3c shows a gradual increase of the width of the π^* peak and a conspicuous emergence of the pre-edge gap state (inset). These trends as a function of temperature coincide with the shifting of the XPS core-level shifts in C and Sn (Figures 1 and 2) and point to interaction of the benzyl fragment with Au as the origin. Taken together, the evidence obtained from XPS and NEXAFS reveals a consistent picture of the reaction on Au surfaces: benzyltrimethylstannane cleaves to form benzyl and trimethyltin fragments on both Au(111) and Au(110) surfaces. Upon thermal activation, trimethyltin radicals form Au−Sn bonds on both surfaces, resulting in XPS chemical shifts (Figure 1b,c). In contrast, the fate of the benzyl counterpart is substrate-dependent: it forms a surface-stabilized radical on Au(111) with a significant chemical shift in XPS (Figure 2a), while on Au(110) it forms a Au−C bond with a well-coupled gap state near the Fermi level of Au and localized on the bond (Figure 3b). The fact that this state is so close to the Fermi level, as evidenced by the shape of the corresponding NEXAFS peak, and is so well hybridized with the π-orbitals generally attributed to charge transport, evidenced by the π^* peak broadening, demonstrates that the gap state is, in fact, the "gateway" state theorized to explain the special electronic properties of Au−C bonded molecular electronic devices.[9,14]

To understand the role of under-coordinated Au in this process, we turn to DFT-based calculations to probe the preferred binding sites of the cleaved fragments on Au (see SI for details). These calculations show that trimethyltin, being ∼0.4 eV more stable on Au(111) than on the Au adatom, strongly favors binding to the flat Au(111) surface (see Tables S1 and S2). The binding energy for benzyl is 1.87 eV on the favored atop binding site on Au(111) compared to 1.75 eV on the adatom. However, these numbers include vdW contributions to the binding energy of 1.36 eV for the atop geometry (due to the proximity of the benzene ring to the flat surface) and only 0.46 eV for the adatom. Subtracting this vdW contribution shows that the Au−C bond formed on the adatom is much stronger (by ∼0.8 eV) than that on the flat surface. Given these results, we perform DFT-based NEB calculations for this molecule on a Au(111) surface with an adatom to serve as the under-coordinated Au site to probe the mechanism for the formation of the Au−C bond. To compute the minimum energy path starting with the intact molecule on surface geometry and ending with the fragments bound on the

surface, we use the climbing-image nudged elastic band (CI-NEB) method as implemented in VASP.[23] This method guarantees that the maximum energy in the path is a saddle point in the energy surface.

Figure 4a shows the reaction mechanism for the dissociation of the intact molecule on the Au(111) surface with a Au adatom, as obtained using the CI-NEB method. For the initial configuration (image 0), we relax the intact molecule starting at different positions relative to the Au adatom and choose the one with the lowest energy. The lowest-energy geometry has the smallest Sn−Au distance of all relaxed initial position guesses (see Figure S2). Still, charge density difference plots (Figure 4b) show that the majority of charge reorganization occurs at the C nearest to Sn, which we label as C1 (arrow in image 0, Figure 4a). This indicates that the initial interaction between the Au adatom and the intact molecule occurs mainly through Au−C1 interaction. For the final configuration (image 6), we compare the total energies of the system with both benzyl and trimethyltin bound to different sites (adatom and flat Au surface; see Figure S3). We find that, in the final state, benzyl strongly prefers to form covalent Au−C bonds with the adatom site rather than the flat surface (by ∼0.6 eV). Trimethyltin can co-adsorb on the adatom or bind to the flat surface, the former favored slightly (∼0.04 eV). Since the under-coordinated Au adatom is likely to be a reactive site in Au, we consider a final configuration where both trimethyltin and benzyl are bonded to the Au adatom. After obtaining the initial and final configurations, images 1−5 are generated using the CI-NEB method.

The optimized energy path (Figure 4a) shows that the intact molecule drifts so that the Au adatom moves closer to C1 and away from Sn. From the initial state to the transition state, the C1−Au bond reduces from 2.8 to 2.1 Å, while C1−Sn bond increases from 2.2 to 2.7 Å. In image 0 before the transition state, the H's attached to C1 point downward, away from Sn and toward Au, indicating that C1 is sp³-coordinated with one C, two H's, and the Sn. At the transition state, however, the H's attached to C1 point away from Au, indicating that the sp³ coordination for C1 now involves Au instead of Sn. Thus the C1−Sn bond weakens while a C1−Au bond forms at the transition state; the predicted barrier in this reaction is 0.5 eV. This calculated
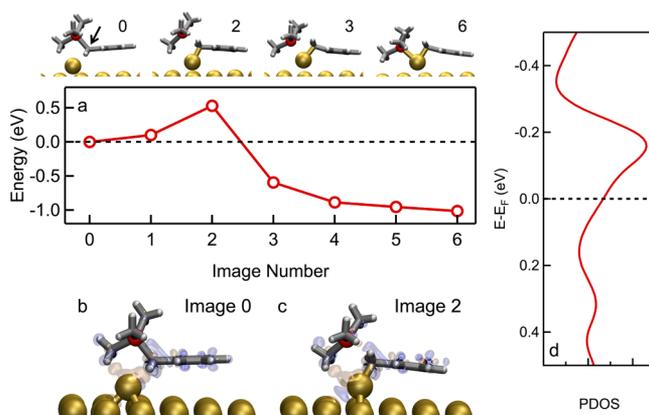
Figure 4. Nudged elastic band calculations on Au(111) + adatom surface. (a) Minimum energy path for dissociation of the intact molecule on Au(111) with an adatom obtained from CI-NEB calculations. Arrow points to atom C1 in image 0. (b,c) Charge density difference plots calculated for (b) image 0 relative to isolated Au slab and isolated molecule and (c) the transition state, image 2. (d) Projected density of states on atom C1.

trajectory emphasizes the fact that Au attacks the benzylic carbon (C1) and not the Sn atom. We attribute the fact that the C1−Sn bond is cleaved rather than any of the three methyl carbons to the energy gained due to resonance stabilization in the aromatic benzylic fragment. Calculation of charge density difference (Figure 4c) of the transition state, image 2, shows Au−C1 bonding in the transition state by hybridization of d_{z^2} orbital of Au adatom with p_z orbital of C1. The fact that C1 is the active site in the reaction is consistent with our observation that binding between the intact molecule and the Au adatom takes place between Au and C1 (instead of Au and Sn). This is in contrast to previous reports of Au−Sn bond formation in solution-phase chemistry carried out in ambient conditions.[24] Finally, analysis of the projected density of states on atom C1 (Figure 4d) shows a significant density around E_{Fermi}, consistent with NEXAFS results showing a new hybridized state close to the Fermi edge.

The above NEB calculation readily explains the facile cleavage of Sn−C1 bonds and formation of Au−C1 bonds on Au(110), a surface characterized by highly under-coordinated ridge sites. On the Au(111) surface, experiments do not evidence the formation of the Au−C bond, despite demonstrating clearly that the molecule cleaves on this surface even at −110 °C. To understand the difference between these surfaces, we first note that, on the Au(110) surface, the benzene ring tilts toward the Au surface as we go from image 2 to 6 in Figure 4a. This tilt also allows the C1−Au bond to achieve the distance and angle necessary for its sp^3 configuration. In contrast, on a Au(111) surface without the adatom, the π-system of the benzene ring lies flat on Au to maximize the energy gained from π−Au interactions and cannot tilt to enable the formation of an sp^3 C1−Au bond. This restricts the orientation of the C1 carbon relative to the Au surface and prevents the formation of the covalent bond on Au(111).

In summary, we have shown that Sn−C bonds in benzyltrimethylstannane are cleaved by Au surfaces. We show through XPS and NEXAFS studies that Au−C bonds are formed only on under-coordinated Au surfaces. Importantly, we find direct evidence for a new electronic state near the Fermi energy, similar to the gateway states hypothesized in previous literature.[9] Finally, we use DFT-NEB to gather a detailed understanding of the reaction pathway for the formation of Au−C bonds on Au surfaces. These results together provide a general understanding of this reaction that can be used to engineer new molecule−metal interfaces and molecular devices incorporating direct Au−C bonds.

ASSOCIATED CONTENT

Ⓢ Supporting Information

Experimental and theoretical methods, additional details, and supporting data. This material is available free of charge via the Internet at http://pubs.acs.org.

AUTHOR INFORMATION

Corresponding Authors
phyqsy@nus.edu.sg
morgante@iom.cnr.it
lv2117@columbia.edu

Notes
The authors declare no competing financial interest.

ACKNOWLEDGMENTS

REFERENCES

(1) Fischer, D.; Curioni, A.; Andreoni, W. *Langmuir* **2003**, *19*, 3567−3571.

(2) Hakkinen, H. *Nat. Chem.* **2012**, *4*, 443−455.

(3) (a) Love, J. C.; Estroff, L. A.; Kriebel, J. K.; Nuzzo, R. G.; Whitesides, G. M. *Chem. Rev.* **2005**, *105*, 1103−1169. (b) Ulman, A. *Chem. Rev.* **1996**, *96*, 1533−1554.

(4) (a) Li, C.; Pobelov, I.; Wandlowski, T.; Bagrets, A.; Arnold, A.; Evers, F. *J. Am. Chem. Soc.* **2008**, *130*, 318−326. (b) Rodriguez, J. A.; Dvorak, J.; Jirsak, T.; Liu, G.; Hrbek, J.; Aray, Y.; Gonzalez, C. *J. Am. Chem. Soc.* **2003**, *125*, 276−285.

(5) Basch, H.; Cohen, R.; Ratner, M. A. *Nano Lett.* **2005**, *5*, 1668−1675.

(6) Yu, M.; Bovet, N.; Satterley, C. J.; Bengio, S.; Lovelock, K. R. J.; Milligan, P. K.; Jones, R. G.; Woodruff, D. P.; Dhanak, V. *Phys. Rev. Lett.* **2006**, *97*, No. 166102.

(7) Schoenfisch, M. H.; Pemberton, J. E. *J. Am. Chem. Soc.* **1998**, *120*, 4502−4513.

(8) Venkataraman, L.; Klare, J. E.; Tam, I. W.; Nuckolls, C.; Hybertsen, M. S.; Steigerwald, M. L. *Nano Lett.* **2006**, *6*, 458−462.

(9) Cheng, Z. L.; Skouta, R.; Vazquez, H.; Widawsky, J. R.; Schneebeli, S.; Chen, W.; Hybertsen, M. S.; Breslow, R.; Venkataraman, L. *Nat. Nanotechnol.* **2011**, *6*, 353−357.

(10) (a) Laurentius, L.; Stoyanov, S. R.; Gusarov, S.; Kovalenko, A.; Du, R. B.; Lopinski, G. P.; McDermott, M. T. *ACS Nano* **2011**, *5*, 4219−4227. (b) Ricci, A. M.; Calvo, E. J.; Martin, S.; Nichols, R. J. *J. Am. Chem. Soc.* **2010**, *132*, 2494−2495.

(11) Zhang, S.; Chandra, K. L.; Gorman, C. B. *J. Am. Chem. Soc.* **2007**, *129*, 4876−4877.

(12) Scholz, F.; Kaletova, E.; Stensrud, E. S.; Ford, W. E.; Kohutova, A.; Mucha, M.; Stibor, I.; Michl, J.; von Wrochem, F. *J. Phys. Chem. Lett.* **2013**, *4*, 2624−2629.

(13) Hong, W.; Li, H.; Liu, S.-X.; Fu, Y.; Li, J.; Kaliginedi, V.; Decurtins, S.; Wandlowski, T. *J. Am. Chem. Soc.* **2012**, *134*, 19425−19431.

(14) Chen, W.; Widawsky, J. R.; Vazquez, H.; Schneebeli, S. T.; Hybertsen, M. S.; Breslow, R.; Venkataraman, L. *J. Am. Chem. Soc.* **2011**, *133*, 17160−17163.

(15) Widawsky, J. R.; Chen, W.; Vazquez, H.; Kim, T.; Breslow, R.; Hybertsen, M. S.; Venkataraman, L. *Nano Lett.* **2013**, *13*, 2889−2894.

(16) Batra, A.; Darancet, P.; Chen, Q.; Meisner, J. S.; Widawsky, J. R.; Neaton, J. B.; Nuckolls, C.; Venkataraman, L. *Nano Lett.* **2013**, *13*, 6233−6237.

(17) Henkelman, G.; Uberuaga, B. P.; Jonsson, H. *J. Chem. Phys.* **2000**, *113*, 9901−9904.

(18) Floreano, L.; Naletto, G.; Cvetko, D.; Gotter, R.; Malvezzi, M.; Marassi, L.; Morgante, A.; Santaniello, A.; Verdini, A.; Tommasini, F.; Tondello, G. *Rev. Sci. Instrum.* **1999**, *70*, 3855−3864.

(19) (a) Taylor, J. A.; Merchant, S. M.; Perry, D. L. *J. Appl. Phys.* **1995**, *78*, 5356−5361. (b) Bancroft, G. M.; Adams, I.; Lampe, H.; Sham, T. K. *J. Electron Spectrosc. Relat. Phenom.* **1976**, *9*, 191−204.

(20) Bjork, J.; Hanke, F.; Stafstrom, S. *J. Am. Chem. Soc.* **2013**, *135*, 5768−5775.

(21) Laforgue, A.; Addou, T.; Belanger, D. *Langmuir* **2005**, *21*, 6855−6865.

(22) Stöhr, J. *NEXAFS spectroscopy*; Springer: Berlin, 1992; Vol. 25.

(23) Sheppard, D.; Terrell, R.; Henkelman, G. *J. Chem. Phys.* **2008**, *128*, No. 134106.

(24) Khobragade, D.; Stensrud, E. S.; Mucha, M.; Smith, J. R.; Pohl, R.; Stibor, I.; Michl, J. *Langmuir* **2010**, *26*, 8483−8490.